Chemical Physics Letters 805 (2022) 139941

Contents lists available at ScienceDirect

Chemical Physics Letters

journal homepage: www.elsevier.com/locate/cplett

Vibrational wave packet dynamics of H_2O^+ and H_2O by strong-field Fourier transform spectroscopy

Hiroyuki Kageyama [a], Tamás Szidarovszky [b,c], Toshiaki Ando [a], Atsushi Iwasaki [a], Attila G. Császár [c,d], Kaoru Yamanouchi [a,*]

[a] Department of Chemistry, School of Science, The University of Tokyo, Japan
[b] Institute of Chemistry, ELTE Eötvös Loránd University, Budapest, Hungary
[c] MTA-ELTE Complex Chemical Systems Research Group, Budapest, Hungary
[d] Laboratory of Molecular Structure and Dynamics, Institute of Chemistry, ELTE Eötvös Loránd University, Budapest, Hungary

A B S T R A C T

The vibrational wave packet dynamics of H_2O^+ and H_2O are investigated by pump–probe measurements using few-cycle intense laser pulses. By a Fourier transform (FT) of the time-dependent yields of the two-body Coulomb explosion pathway, $H_2O^{2+} \rightarrow H^+ + OH^+$, and the parent ion, H_2O^+, the vibrational excitation processes in the electronic ground states of H_2O^+ and H_2O induced by the intense laser field are retrieved from the phases of the respective vibrational peaks in the FT spectrum. Accurate quantum-dynamics simulations on H_2O^+ confirm both the peak assignment and the origin of the time-dependent ionization yields of the vibrational wave packet.

1. Introduction

Recent advances in ultrashort-pulsed laser technologies have enabled us to perform pump–probe measurements to investigate ultrafast molecular dynamics in real time [1–4]. Thanks to the broad bandwidth and short duration of the ultrashort laser pulses, a coherent superposition of vibrational and/or rotational eigenstates is created by the irradiation of a molecule with a pump laser pulse, so that the temporal evolution of the wave packet is monitored by a probe laser pulse. Using sub-10 fs laser pulses, even the fastest vibrational motion of H_2 and D_2 [1] whose vibrational periods are of the order of 10 fs can be probed.

By the pump–probe measurements, we can probe the temporal evolution of the vibrational and/or rotational wave packet created by a pump pulse in real time for a long period of time in the absence of an optical field, and consequently, we can retrieve frequency-domain information by the Fourier transform (FT) of the variation of the pump–probe signals in the time domain [5,6]. As shown in our recent studies [7,8], by lengthening the pump–probe time-delay range, we can determine the vibrational level separations of neutral molecules and molecular cations as well as the atomic energy levels with ultrahigh frequency resolution. It should be emphasized that, from the FT of the time-domain signals, not only the frequencies of the oscillation but also the phases of the created wave packet can be extracted.

In the present study, we investigate the vibrational dynamics of H_2O and H_2O^+ by pump–probe measurements using few-cycle intense laser pulses. By monitoring the time-dependent yield of the two-body Coulomb explosion pathway, $H_2O^{2+} \rightarrow H^+ + OH^+$, as well as the time-dependent yield of H_2O^+, we extract not only the frequencies of the vibrational modes of H_2O and H_2O^+ but also their initial phases, carrying the information on how the vibrational wave packet is created within a molecule. We also perform high-accuracy vibrational quantum dynamics simulations, showing good agreement with the experimental results, to confirm the interpretation of the vibrational dynamics based on the experimental data.

2. Experimental

The output of a Ti:sapphire laser system (repetition rate: 5 kHz, pulse energy: 0.5 mJ, central wavelength: 800 nm, pulse duration: 30 fs) was focused into a hollow-core fiber (inner diameter: 330 μm, length: 1.5 m) filled with an Ar gas to broaden the spectral bandwidth through the self-phase modulation. The few-cycle laser pulses were generated by the dispersion compensation of the output of the hollow-core fiber using chirped mirrors and a pair of wedge plates. The few-cycle laser pulses whose duration was measured to be ~ 6 fs were introduced into a Michelson interferometer for producing pump and probe laser pulses. The time delay, Δt, between the pump and probe laser pulses was varied

* Corresponding author.
E-mail address: kaoru@chem.s.u-tokyo.ac.jp (K. Yamanouchi).

https://doi.org/10.1016/j.cplett.2022.139941
Received 18 May 2022; Accepted 5 August 2022
Available online 10 August 2022

up to 1600 fs using an optical stage in the interferometer. The time delay introduced by the optical stage was measured using a He-Ne laser.

The pump and probe laser pulses were introduced into an ultrahigh vacuum chamber and focused on an effusive molecular beam of a water vapor by a concave mirror ($f = 150$ mm) in the vacuum chamber. The peak intensity at the focus was estimated to be $\sim 2 \times 10^{14}$ W cm^{-2} for both the pump and probe laser pulses. The parent and fragment ions were accelerated by the electrodes and detected by a delay-line detector (Hex120 Roentdek GmbH). Three-dimensional momentum vectors of the ions were obtained from their position and time-of-flight at the detector.

3. Results and discussion

3.1. Dissociating and bound wave packet of H_2O^+ and H_2O

We extract the events accompanied by the two-body Coulomb explosion pathway, $H_2O^{2+} \rightarrow H^+ + OH^+$, by imposing the coincidence conditions that the sum of the momenta of the two fragments is nearly equal to zero. Fig. 1 shows the distribution of the kinetic energy release (KER) of this pathway as a function of the pump–probe time delay, Δt. The intense signal at $\Delta t = 0$ fs represents an enhancement of the yield of the double ionization of H_2O due to the temporal overlap of the pump and probe laser pulses. The weak side-peak structures appearing at around $\Delta t = \pm 65$ fs can be ascribed to the interference originating from the small spike-like structures in the tail part of the laser intensity profile, which was confirmed by the two-dimensional spectral shearing interferometry (2DSI) measurements [9].

The time-delay dependence of the KER distribution shown in Fig. 1 exhibits two major components, that is, one horizontal and broad component whose central KER is around 6.0 eV in the entire time-delay range up to 1600 fs and the other component whose KER decreases rapidly to ~ 1 eV by around $\Delta t = 250$ fs and reaches ~ 0.5 eV at 1600 fs with a narrow KER distribution. The horizontal and broad KER distribution whose peak is located at 5.8 eV is consistent with the KER distributions reported previously for the decomposition of H_2O^{2+} prepared by the Franck-Condon projection to H_2O^{2+} from H_2O or from H_2O^+ [11,12]. Because this peak profile does not vary in the entire time-delay range, the horizontal and broad KER distribution can be assigned to the Coulomb explosion process, $H_2O^{2+} \rightarrow H^+ + OH^+$, induced by the double ionization of H_2O by the pump and probe pulses.

The component whose KER decreases as Δt increases represents the dissociation of H_2O^+ created by the pump pulse, which is ionized further into H_2O^{2+} by the probe pulse, leading to the Coulomb explosion into $H^+ + OH^+$. This component representing the dissociation of H_2O^+ exhibits a tail extending towards the larger KER side in the asymptotic region, which is consistent with the previous observation of the dissociation of the electronically excited $\tilde{B}\ ^2B_2$ state of D_2O^+ by the PEPICO method [13] and can be interpreted as the temporal evolution of the dissociating wave packet of H_2O^+ prepared in the $\tilde{B}\ ^2B_2$ state above the dissociation threshold of H(1s) + $OH^+(X\ ^3\Sigma^-)$ of H_2O^+.

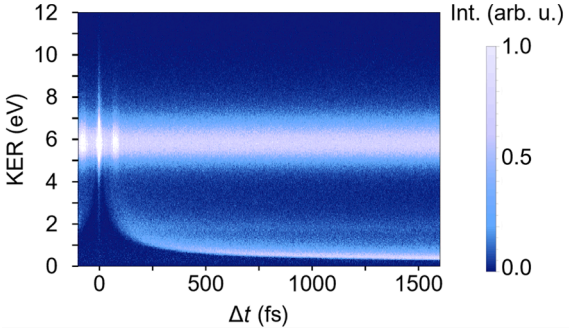

Fig. 1. The KER distribution of the Coulomb explosion pathway $H_2O^{2+} \rightarrow H^+ + OH^+$ plotted as a function of the pump–probe time delay Δt. The color scale is saturated at $\Delta t = 0$ and $\Delta t = \pm 65$ fs. A weak horizontal distribution whose peak is located at ~ 1.9 eV, which starts appearing at the time delay of $\Delta t \sim 200$ fs continues until the asymptotic region of $\Delta t = 1600$ fs, represents the dissociation proceeding in the neutral manifold of H_2O, $H_2O(\tilde{A}\ ^1B_1) \rightarrow H(1s) + OH(X\ ^2\Pi, v = 0 - 4)$ [10] induced by the five-photon excitation to the $\tilde{A}\ ^1B_1$ state of H_2O by the pump pulse.

3.2. Vibrational dynamics of the bound wave packet of H_2O^+

The time-delay dependence of the yield of the Coulomb explosion pathway, $H_2O^{2+} \rightarrow H^+ + OH^+$, in the KER range of 4–8 eV is shown in Fig. 2(a), which exhibits fine oscillations in the entire time-delay range up to $\Delta t = 1600$ fs. The inset of Fig. 2(a), which is obtained by the subtraction of the base line component in Fig. 2(a) in the time-delay range of $\Delta t \geq 200$ fs, exhibits a complex oscillatory pattern. The FT of the inset of Fig. 2(a) is shown in Fig. 2(b), in which two prominent peaks can be found at 1414 and 3214 cm^{-1} and a smaller peak at 3656 cm^{-1}. The frequencies in the FT spectrum are calibrated using the vibrational level spacing of H_2^+ in the electronic ground state obtained by the FT of the time-delay dependence of the yield of H^+ originating from the residual H_2 gas in the vacuum chamber.

In order to obtain the positions, amplitudes, and phases of the peaks in Fig. 2(b), we adopt a sinc-type fitting function [7] given by

$$F[k] = P\exp\left[i\left(\pi\frac{\tilde{\nu} - \tilde{\nu}_0}{\Delta\tilde{\nu}} + \phi\right)\right]\mathrm{sinc}\left(\pi\frac{\tilde{\nu} - \tilde{\nu}_0}{\Delta\tilde{\nu}}\right), \quad (1)$$

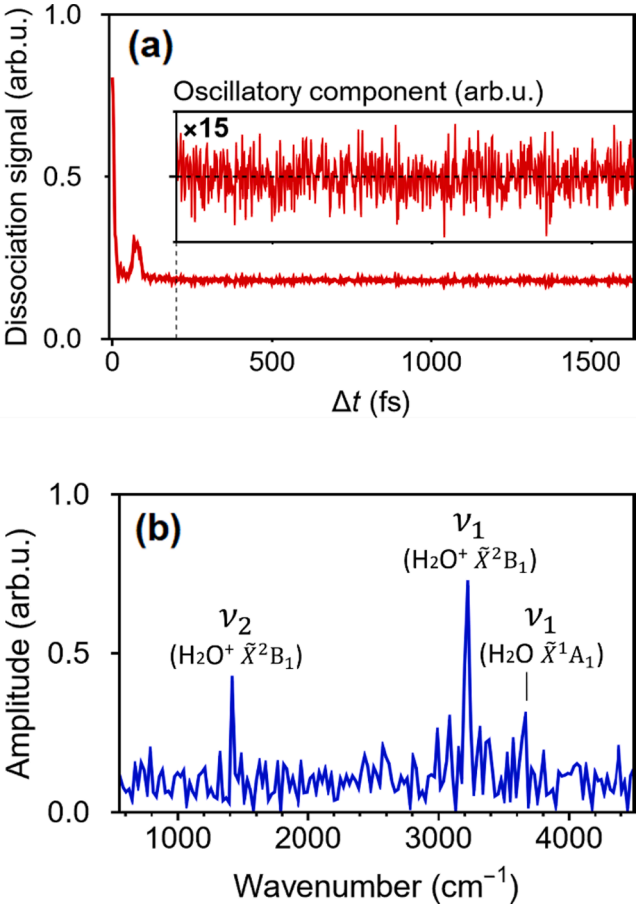

Fig. 2. (a) The time-delay dependence of the yield of the Coulomb explosion pathway, $H_2O^{2+} \rightarrow H^+ + OH^+$, with $4 \leq KER \leq 8$ eV. The inset shows the extracted oscillatory component of the yield. (b) The FT spectrum obtained by discrete Fourier transform of the oscillatory component in the time-delay range of 200 fs $< \Delta t <$ 1600 fs.

where the three fitting parameters P (>0), $\widetilde{\nu}_0$, and ϕ represent the amplitude, the wavenumber of the peak position, and the phase, respectively. The denominator in the sinc function, $\Delta\widetilde{\nu}$, is the wavenumber separation between adjacent bins. Least-squares fits are performed for both the real and imaginary parts of the peak profiles. The initial phase of the oscillation at $\Delta t = 0$ fs is obtained by

$$\phi_0 = -\left(\phi + 2\pi \frac{n_0}{N}\frac{\widetilde{\nu}_0}{\Delta\widetilde{\nu}}\right), \tag{2}$$

where n_0 is the data length between the position of $\Delta t = 0$ fs and the beginning position of the input data and N is the length of the input data. The frequencies and initial phases of the three peaks appearing in Fig. 2 (b) obtained by the least-squares fit are listed in Table 1.

As summarized in Table 1, the peaks appearing at 1414 and 3214 cm^{-1} can be assigned respectively to the ν_1 (symmetric stretching) (=3212.86 cm^{-1} [14]) and ν_2 (bending) (=1408.42 cm^{-1} [15]) vibrational modes of the $\widetilde{X}\ ^2B_1$ state of H_2O^+ and the peak appearing at 3656 cm^{-1} can be assigned to the ν_1 (symmetric stretching) vibrational mode (=3657.05 cm^{-1} [16]) of the $\widetilde{X}\ ^1A_1$ state of neutral H_2O.

These observations indicate that the pump laser pulses create coherently the vibrational wave packet composed of the vibrational levels of H_2O^+ as well as the vibrational wave packet of H_2O, both of which evolve in time. Because both the ionization rate of H_2O^+ to H_2O^{2+} by the probe pulse and the double ionization rate of H_2O to H_2O^{2+} by the probe pulse vary depending on the position of the vibrational wave packet of H_2O^+ as well as on that of H_2O, the yield of H_2O^{2+} leading to the Coulomb explosion process, $H_2O^{2+} \rightarrow H^+ + OH^+$, is expected to oscillate at the vibrational frequencies of both H_2O^+ and H_2O.

3.3. Quantum dynamics simulations

In order to support the interpretation of the experimental results, we perform simulations of the propagation of the vibrational wave packet of H_2O^+ and converted the results to a spectrum corresponding to the observed FT spectrum. In the simulation, we neglect molecular rotation and assume an instantaneous ionization by the pump pulse, *i.e.*, the vibrational ground state wave function, $|000\rangle \equiv |\phi_{000}^{H_2O}\rangle$, of the $\widetilde{X}\ ^1A_1$ state of neutral H_2O is projected onto the potential energy surface (PES) of the $\widetilde{X}\ ^2B_1$ state of H_2O^+ according to the Franck-Condon principle. The projected wave function, $|\phi_{000}^{H_2O}\rangle$, which is no longer a stationary state on the PES of H_2O^+, starts evolving in time as a vibrational wave packet.

The first step of the simulation is the computation of vibrational wave functions for H_2O and H_2O^+. For this purpose, we employ the variational triatomic nuclear-motion code D^{2}FOPI [17] using the PESs of H_2O [18,19] and H_2O^+ [20]. By these computations, we obtain the wave function of the vibrational ground state of neutral H_2O in the electronic ground state, $|\phi_{000}^{H_2O}\rangle$, and a few tens of vibrational wave functions, $|v_1v_2v_3\rangle \equiv |\phi_{v_1v_2v_3}^{H_2O^+}\rangle$, of H_2O^+ cation in the electronic ground state and confirm that the vibrational level energies match the corresponding experimental values of H_2O^+ within 10 cm^{-1} [20].

In the second step, we calculate the projection of $|\phi_{000}^{H_2O}\rangle$ to $|\phi_{v_1v_2v_3}^{H_2O^+}\rangle$ given by

$$\left\langle \phi_{v_1v_2v_3}^{H_2O^+} \middle| \phi_{000}^{H_2O} \right\rangle \equiv C_{v_1v_2v_3}^{000}. \tag{3}$$

Using these projections, we construct the initial wave packet,

$$|\Psi(0)\rangle = \sum_{v_1,v_2,v_3} C_{v_1v_2v_3}^{000} \left| \phi_{v_1v_2v_3}^{H_2O^+} \right\rangle, \tag{4}$$

on the cationic PES, which evolves in time as

$$|\Psi(t)\rangle = \sum_{v_1,v_2,v_3} C_{v_1v_2v_3}^{000} e^{-\frac{i}{\hbar}E_{v_1v_2v_3}t} \left| \phi_{v_1v_2v_3}^{H_2O^+} \right\rangle, \tag{5}$$

where $E_{v_1v_2v_3}$ represents the energy of $|\phi_{v_1v_2v_3}^{H_2O^+}\rangle$.

In the third and final step of the simulation, the time evolution of a given physical quantity $\widehat{A}$ is computed as

$$\langle \widehat{A} \rangle (t) = \langle \Psi(t) | \widehat{A} | \Psi(t) \rangle \tag{6}$$

The physical quantities whose temporal evolutions are computed according to Eq. (6), are the O–H internuclear distance, R_{OH}, of H_2O^+, the cosine of the H–O–H bond angle, θ, of H_2O^+, and $w_{ADK}(R_{OH}, \cos\theta)$, representing the coordinate-dependent ionization rates from H_2O^+ ($\widetilde{X}\ ^2B_1$) to the lowest singlet and triplet electronic states of H_2O^{2+}, computed using a simple isotropic Ammosov-Delone-Krainov (ADK) formula [21] with the PES values calculated at the CCSD(T)/aug-cc-pVQZ level [22–24] using the GAUSSIAN code [25].

As can be seen in the two-dimensional ionization rate, $w_{ADK}(R_{OH}, \cos\theta)$, shown in Fig. 3, the probability of the ionization to the lowest triplet electronic state of H_2O^{2+} is one order of magnitude larger than the probability of the ionization to the lowest singlet state. Therefore, hereafter, only the ionization to the triplet state is discussed. It can also be seen in Fig. 3 that ionization occurs preferentially when $\cos(\theta)$ and R_{OH} increase simultaneously.

3.4. Experimental and theoretical FT spectra

The FT of the simulated time-dependent expectation value of the two-dimensional ADK ionization rate of H_2O^+, $w_{ADK}(R_{OH}, \cos\theta)$, is

Table 1
The vibrational energy separations and the initial phases of the electronic ground $\widetilde{X}\ ^2B_1$ state of H_2O^+ and the electronic ground $\widetilde{X}\ ^1A_1$ state of H_2O obtained by the FT spectrum of the yield of the Coulomb explosion pathway, $H_2O^{2+} \rightarrow H^+ + OH^+$, and the yield of H_2O^+ with the observed values of the vibrational energy separations reported in Refs. [14–16].

	Assignment ($v_1v_2v_3'$)-($v_1v_2v_3$)	Vibrational energy /cm^{-1}	Initial phase / π rad	Observed values /cm^{-1}
H_2O^+	(100)-(000)	3214(1) [a]	–0.85(6) [a]	3212.86 (Ref. [14])
	(010)-(000)	1414(3) [a]	0.94(12) [a]	1408.42 (Ref. [15])
H_2O	(100)-(000)	3656(3) [a]	–0.60(14) [a]	3657.05 (Ref. [16])
	(100)-(000)	3662(4) [b]	–0.69(7) [b]	

a) Determined from the FT spectrum shown in Fig. 2(b).
b) Determined from the FT spectrum shown in Fig. 5(b).

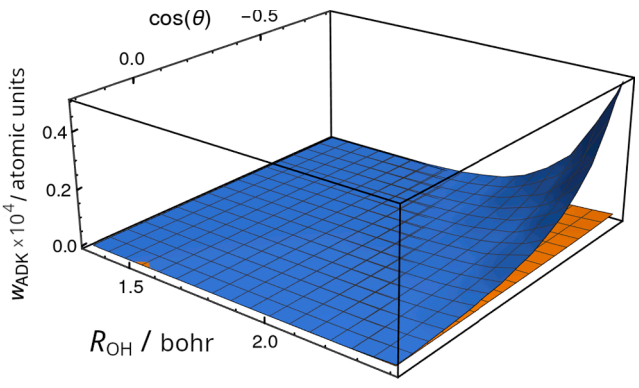

Fig. 3. The ADK ionization rates of H_2O^+ as a function of $\cos(\theta)$ and R_{OH}, where θ is the H–O–H bond angle and R_{OH} represents the O–H internuclear distance in the symmetric stretch mode. The orange and blue surfaces are responsible for the pathways in which H_2O^{2+} is produced in its lowest-lying singlet and triplet electronic states, respectively.

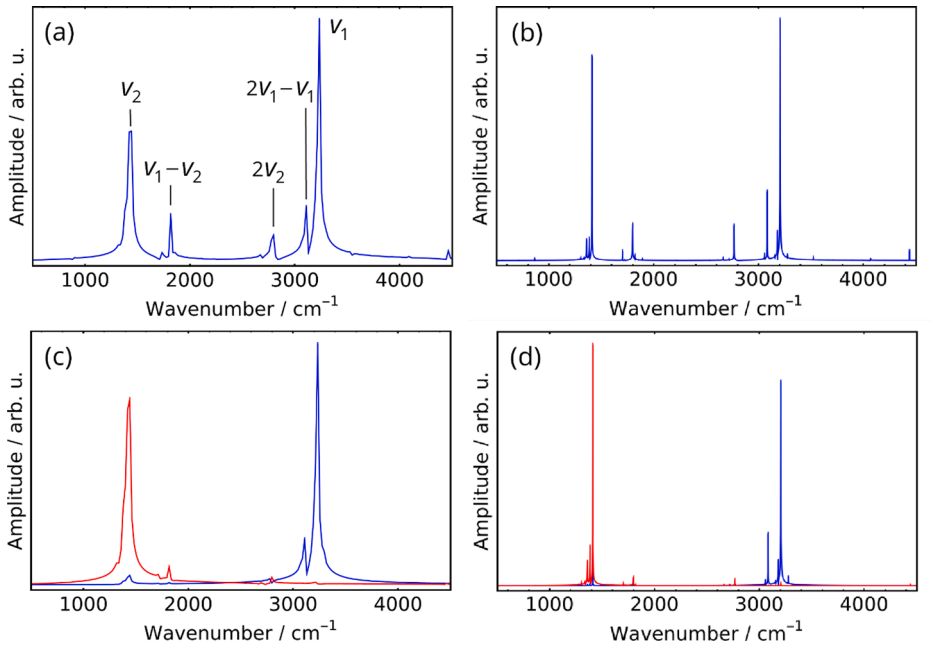

Fig. 4. (a) The Fourier transform (FT) of the $w_{ADK}(t)$ expectation value of the ADK ionization rate from H_2O^+ to the lowest triplet electronic state of H_2O^{2+}. (b) Same as in (a) for the simulation time of 16000 fs. (c) Theoretical FT spectra obtained using the time evolutions of $\langle R_{OH}\rangle$ (blue line) and $\langle\cos\theta\rangle$ (red line) of H_2O^+ for the simulation time of 1600 fs. (d) Same as in (c) for the simulation time of 16000 fs.

shown in Fig. 4(a). The positions and intensities of the two peaks in the theoretical FT spectrum are in good agreement with those in the experimental FT spectrum shown in Fig. 2(b), which confirms that the time-delay dependence of the yield of the Coulomb explosion pathway shown in Fig. 2(a) represents the temporal evolution of the vibrational wave packet prepared in the bound well of the $\tilde{X}\ ^2B_1$ state of H_2O^+.

In order to confirm the assignments of the two peaks appearing at 1414 and 3214 cm^{-1} in the FT spectrumshown in Fig. 2(b), we perform wave packet propagation on the three-dimensional potential energy surface (PES) of the $\tilde{X}\ ^2B_1$ state of H_2O^+. First, an initial wave packet prepared by assuming instantaneous ionization is propagated on the PES. Then, the temporal variation of the expectation value of the O–H internuclear distance R_{OH} of H_2O^+, $\langle R_{OH}\rangle$, and that of the expectation value of the cosine of the H–O–H bond angle of H_2O^+, $\langle\cos\theta\rangle$, are Fourier transformed. The resultant FT spectra are shown in Fig. 4(b). The sharp peak at 3203 cm^{-1} in the FT spectrum in Fig. 4(c) obtained by the variation of $\langle R_{OH}\rangle$ confirms the assignment of the corresponding peak in Figs. 2(b) and 4(a) to the symmetric stretching (ν_1) mode of the $\tilde{X}\ ^2B_1$ state of H_2O^+ and the sharp peak at 1407 cm^{-1} in the FT spectrum in Fig. 4(c) obtained by the variation of $\langle\cos\theta\rangle$ confirms the assignment of the corresponding peak in Figs. 2(b) and 4(a) to the bending (ν_2) mode of the $\tilde{X}\ ^2B_1$ state of H_2O^+. The simulated FT spectra also predict the ν_1-ν_2, $2\nu_2$, and $2\nu_1$-ν_1 peaks at 1796 cm^{-1}, 2765 cm^{-1}, and 3081 cm^{-1}, respectively, as shown in Fig. 4(a) and 4(b). These peaks have much smaller intensity than the ν_1 and ν_2 peaks, and they cannot be identified clearly in the experimental spectrum of Fig. 2(b). As demonstrated in Fig. 4(b) and 4(d), as the propagation time increases to 16000 fs, which is ten times as long as the propagation time for Fig. 4(a) and 4(c), the higher frequency resolution of the FT spectrum can be achieved.

As listed in Table 1, the initial phases of the two peaks assigned to the vibrational frequencies of H_2O^+ are close to π. Because the O–H bond length and the H–O–H bond angle at the equilibrium structure in the $\tilde{X}\ ^1A_1$ state of H_2O (R_{OH} = 0.95782 Å and θ_{HOH} = 104.485° [26]) are smaller to a certain extent than those in the $\tilde{X}\ ^2B_1$ state of H_2O^+ (R_{OH} = 0.9992 Å and θ_{HOH} = 109.30° [14]), the initial vibrational wave packet prepared on the PES of H_2O^+ from H_2O will start propagating towards the longer bond length and larger bond angle regions. Considering that the ionization rate of H_2O^+ to H_2O^{2+} increases when the O–H bond length increases as well as when the H–O–H bond angle increases as shown in Fig. 4, the yield of H_2O^{2+} is expected to increase. Consequently, the yield of the Coulomb explosion pathway is expected to increase when the wave packet reaches the outer turning point of the bound potential along the symmetric stretching coordinate as well as that along the bending coordinate. Because a phase π is expected to be incremented by the time when the wave packet reaches the outer turning points after its creation, the initial phase of π reflects this ionization enhancement at the outer turning points on the PES of H_2O^+.

3.5. *Vibrational excitation in neutral H_2O*

The appearance of the peak at 3656 cm^{-1}, corresponding to the ν_1 fundamental of the $\tilde{X}\ ^1A_1$ state of H_2O, in Fig. 2(b) shows that the pump laser pulses also play a role in the vibrational excitation of neutral H_2O. As listed in Table 1, the initial phase of this peak in the FT spectrum, $-0.60(14)\pi$, is significantly different from the initial phases obtained for the two peaks assigned to the vibrational modes of H_2O^+.

As has been discussed in Refs. [27–30], there are mainly-two mechanisms by which a vibrational wave packet is prepared in neutral molecules by the irradiation of an ultrashort intense laser pulse. One is the *R*-selective depletion, and the other is the bond softening. In the *R*-selective depletion mechanism, molecules having the shorter or longer bond length tend to be more efficiently ionized, resulting in the formation of a wave packet in the neutral manifold, resulting in the ion-yield oscillation with an initial phase of -π. In the bond softening mechanism, a vibrational wave packet with an initial phase of -π/2 is created when the ionization proceeds more efficiently at the longer bond length while a vibrational wave packet with an initial phase of π/2 is created when the ionization proceeds more efficiently at the shorter bond length. The experimentally obtained initial phase, $-0.60(14)\pi$, which is close to -π/2, suggests that the dominant mechanism of the vibrational excitation in H_2O is the bond softening and that the ionization rate becomes larger when the O–H bond becomes longer.

In order to examine the initial phase in the neutral manifold, we

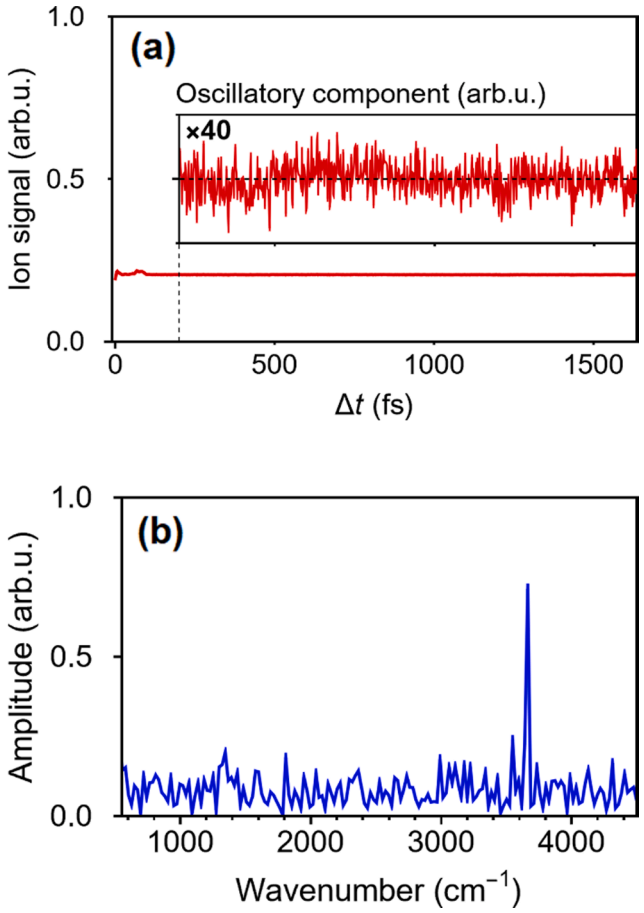

Fig. 5. (a) The time-dependent yield of the parent ion, H_2O^+. The inserted figure shows the extracted oscillatory component of the yield. **(b)** The FT spectrum obtained by performing discrete Fourier transform of the oscillatory component shown in Fig. 5(a) for $\Delta t \geq 200$ fs.

record the dependence of the yield of H_2O^+ on the pump–probe time delay as shown in Fig. 5(a), and then, perform an FT. In the resultant FT spectrum shown in Fig. 5(b), a sharp peak can be identified at 3662 cm^{-1}, corresponding to the frequency of the ν_1 fundamental of the $\tilde{X}\ ^1A_1$ state of H_2O, and the initial phase of this peak is determined to be $-0.69(7)\pi$, which is consistent with the initial phase, $-0.60(14)\pi$, obtained above for the peak in Fig. 2(b) assigned to the ν_1 mode of the $\tilde{X}\ ^1A_1$ state of H_2O. The appearance of the ν_1 mode of the $\tilde{X}\ ^1A_1$ state of H_2O in the FT spectrum in Fig. 5(b) shows that the ionization rate of H_2O to H_2O^+ by the probe laser pulse is modulated by the motion of the wave packet created in H_2O by the pump pulse through the bond-softening mechanism.

4. Summary

The vibrational wave packet dynamics of H_2O^+ and H_2O in their electronic ground states have been investigated by pump–probe measurements using few-cycle intense laser pulses and accurate quantum-dynamics simulations on H_2O^+. By a Fourier transform (FT) of the time-dependent yield of the two-body Coulomb explosion pathway, $H_2O^{2+} \rightarrow H^+ + OH^+$, and that of the parent ion, H_2O^+, the vibrational fundamentals of $\nu_1 = 3214(1)$ cm^{-1} and $\nu_2 = 1414(3)$ cm^{-1} are obtained for H_2O^+, and $\nu_1 = 3662(1)$ cm^{-1} for H_2O. The vibrational excitation processes of H_2O^+ and H_2O induced by the intense laser field are retrieved from the phases of the respective vibrational peaks in the FT spectrum. The high-accuracy quantum dynamics simulations performed on H_2O^+ have verified the assignment of the experimental peaks and their origins based on the time-dependent ionization yields of the vibrational wave packets. As has been demonstrated in the present study, by pump–probe FT spectroscopy using ultrashort intense laser pulses, we are able to determine vibrational fundamentals of molecules and molecular cations and discuss how the created vibrational wave packets evolve on the multi-dimensional potential energy surfaces.

CRediT authorship contribution statement

Hiroyuki Kageyama: Investigation, Writing – original draft. **Tamás Szidarovszky:** Investigation, Software, Writing – original draft. **Toshiaki Ando:** Investigation, Methodology. **Atsushi Iwasaki:** Investigation, Methodology. **Attila G. Császár:** Supervision, Funding acquisition. **Kaoru Yamanouchi:** Conceptualization, Supervision, Funding acquisition, Writing – review & editing.

Declaration of Competing Interest

The authors declare that they have no known competing financial interests or personal relationships that could have appeared to influence the work reported in this paper.

Data availability

Data will be made available on request.

Acknowledgements

One of the co-authors (K. Y.) thanks Prof. Kozo Kuchitsu for his sincere guidance for many years. This work was supported by JSPS-HAS Bilateral Joint Research Projects/Seminars Grant Nos. JPJSBP120203801 and NKM 2019-44. The present research was supported by Grant-in-Aid for Specially Promoted Research (Grant No. JP15H05696), Grant-in-Aid for Scientific Research (A) (Grant No. 20H00371), the János Bolyai Research Scholarship of the Hungarian Academy of Sciences, and NKFIH (Grant No. FK134291 and K138233).

References

[1] T. Ergler, A. Rudenko, B. Feuerstein, K. Zrost, C.D. Schröter, R. Moshammer, J. Ullrich, Phys. Rev. Lett. 97 (2006), 193001.
[2] A. Hishikawa, A. Matsuda, M. Fushitani, E.J. Takahashi, Phys. Rev. Lett. 99 (2007), 258302.
[3] H. Xu, C. Marceau, K. Nakai, T. Okino, S.-L. Chin, K. Yamanouchi, J. Chem. Phys. 133 (2010), 071103.
[4] T. Ando, A. Shimamoto, S. Miura, K. Nakai, H. Xu, A. Iwasaki, K. Yamanouchi, Chem. Phys. Lett. 624 (2015) 78.
[5] T. Ando, A. Shimamoto, S. Miura, A. Iwasaki, K. Nakai, K. Yamanouchi, Commun. Chem. 1 (2018) 7.
[6] T. Ando, A. Iwasaki, K. Yamanouchi, Mol. Phys. 117 (2019) 1732.
[7] T. Ando, A. Iwasaki, K. Yamanouchi, Phys. Rev. Lett. 120 (2018), 263002.
[8] T. Ando, A. Liu, N. Negishi, A. Iwasaki, K. Yamanouchi, Phys. Lev. A 104 (2021), 033516.
[9] J.R. Birge, R. Ell, F.X. Kärtner, Opt. Lett. 31 (2006) 2063.
[10] X.F. Yang, D.W. Hwang, J.J. Lin, X. Ying, J. Chem. Phys. 113 (2000) 10597.
[11] D. Reedy, J.B. Williams, B. Gaire, A. Gatton, M. Weller, A. Menssen, T. Bauer, K. Henrichs, P. Burzynski, B. Berry, Z.L. Streeter, J. Sartor, I. Ben-Itzhak, T. Jahnke, R. Dörner, T. Weber, A.L. Landers, Phys. Rev. A 98 (2018), 053430.
[12] H.B. Pedersen, C. Domesle, L. Lammich, S. Dziarzhytski, N. Guerassimova, R. Treusch, L.S. Harbo, O. Heber, B. Jordon-Thaden, T. Arion, M. Förstel, M. Stier, U. Hergenhahn, A. Wolf, Phys. Rev. A 87 (2013), 013402.
[13] I. Powis, D.J. Reynolds, J. Chem. Soc. Faraday Trans. 87 (1991) 921.
[14] T.R. Huet, C.J. Pursell, W.C. Ho, B.M. Dinelli, T. Oka, J. Chem. Phys. 97 (1992) 5977.
[15] P.R. Brown, P.G. Davies, R.J. Stickland, J. Chem. Phys. 91 (1989) 3384.
[16] D.F. Smith, J. Overend, Spectrochim. Acta A 28 (1972) 471.
[17] T. Szidarovszky, A.G. Császár, G. Czakó, Phys. Chem. Chem. Phys. 12 (2010) 8373.
[18] O.L. Polyansky, A.G. Császár, S.V. Shirin, F.N. Zobov, P. Barletta, J. Tennyson, D. W. Schwenke, P.J. Knowles, Science 299 (2003) 539.
[19] P. Barletta, S.V. Shirin, N.F. Zobov, O.L. Polyansky, J. Tennyson, E.F. Valeev, A. G. Császár, J. Chem. Phys. 125 (2006), 204307.
[20] M. Brommer, B. Weis, B. Follmeg, P. Rosmus, S. Carter, N.C. Handy, H.-J. Werner, P.J. Knowles, J. Chem. Phys. 98 (1993) 5222.
[21] F.A. Ilkov, J.E. Decker, S.L. Chin, J. Phys. B: At. Mol. Opt. Phys. 25 (1992) 4005.

[22] K. Raghavachari, G. Trucks, J. Pople, M. Head-Gordon, Chem. Phys. Lett. 157 (1989) 479.
[23] T. Dunning Jr, J. Chem. Phys. 90 (1989) 1007.
[24] R. Kendall, T. Dunning Jr, R.J. Harrison, J. Chem. Phys. 96 (1992) 6796.
[25] M. J. Frisch et al, Wallingford, CT.: Gaussian, Inc., (2009).
[26] A.G. Császár, G. Czakó, T. Furtenbacher, J. Tennyson, V. Szalay, S.V. Shirin, N. F. Zobov, O.L. Polyansky, J. Chem. Phys. 112 (2005), 214305.
[27] T. Ergler, B. Feuerstein, A. Rudenko, K. Zrost, C.D. Schröter, R. Moshammer, J. Ullrich, Phys. Rev. Lett. 97 (2006), 103004.
[28] Z. Wei, J. Li, L. Wang, S.T. See, M.H. Jhon, Y. Zhang, F. Shi, M. Yang, Z.-H. Loh, Nat. Commun. 8 (2017) 735.
[29] L. Fang, G.N. Gibson, Phys. Rev. Lett. 100 (2008), 103003.
[30] E. Goll, G. Wunner, A. Saenz, Phys. Rev. Lett. 97 (2006), 103003.